Acta Ophthalmologica

Acta Ophthalmologica 2018

Optic nerve head morphology in primary open-angle glaucoma and nonarteritic anterior ischaemic optic neuropathy measured with spectral domain optical coherence tomography

Hemma Resch,[1] Christoph Mitsch,[1] Ivania Pereira,[2] Florian Schwarzhans,[2] Lorenz Wasserman,[1] Anton Hommer,[3] Andreas Reitner[1] and Clemens Vass[1]

[1]Department of Ophthalmology and Optometry, Medical University Vienna, Vienna, Austria
[2]Center for Medical Statistics Informatics and Intelligent Systems, Section for Medical Information Management and Imaging, Medical University Vienna, Vienna, Austria
[3]Hommer Ophthalmology Institute, Vienna, Austria

ABSTRACT.

Purpose: **Optic nerve head (ONH) parameters as well as circumpapillary retinal nerve fibre layer (RNFL) thickness values measured with two different spectral domain optical coherence tomography (SD-OCT) machines (Spectralis® and Cirrus® OCT) have been compared between two patient groups, primary open-angle glaucoma (POAG), nonarteritic anterior ischaemic optic neuropathy (NAION) and healthy controls. A comparison of the performance of the two OCT machines was made.**

Methods: **Twenty healthy controls, 20 POAG and 20 NAION patients with comparable visual field defects were included. Comparison between groups was made using ANOVA and post hoc *t*-tests. To evaluate the diagnostic power of OCT to differentiate POAG from NAION, a stepwise linear regression analysis of the rim-RNFL correlation with adjusting covariates (optic disc area and age) was performed. Based on the regression formula, the area under the receiver operator characteristic (AUROC) was calculated.**

Results: **Both glaucoma and NAION patients showed significantly smaller global RNFL thickness values compared to healthy subjects in *t*-tests ($p < 0.001$), while only patients with glaucoma showed significantly smaller global ONH parameters for both devices compared to healthy subjects ($p < 0.001$). Correlation between global ONH parameters was highly statistically significant ($r = 0.93$), whereas in *t*-test a statistically significant difference between the two machines was detected ($p < 0.001$). Area under the receiver operator characteristic revealed a similarly good discrimination between glaucoma and NAION for Spectralis® (0.980) and Cirrus® OCT (0.945).**

Conclusion: **NAION patients have similar RNFL thickness values as do glaucomatous eyes, whereas ONH parameters in NAION eyes were similar to those seen in healthy controls. This difference might help discriminating between these two different disease conditions in a chronic disease stadium, and in this regard, none of the two OCT machines performed better.**

Key words: Bruch's membrane opening-minimum rim width – nonarteritic anterior ischaemic optic neuropathy – primary open-angle glaucoma – retinal nerve fibre layer – spectral domain optical coherence tomography

Acta Ophthalmol. 2018: 96: e1018–e1024

doi: 10.1111/aos.13804

Introduction

Different optic neuropathies produce to some extent, unspecific changes of the optic nerve head (ONH) and their axons, and the discrimination between ONH diseases can be difficult. Especially, to distinguish between glaucomatous and nonglaucomatous optic neuropathies can be challenging.

Primary open-angle glaucoma (POAG) is characterized by a chronic decline of retinal ganglion cells (RGC) and their axons, which results in thinning of the peripapillary retinal nerve fibre layer (RNFL) and a thinning of the neuroretinal rim which becomes visible through an increased excavation

of the ONH (Quigley et al. 1982). Increased intraocular pressure is the most important risk factor for the disease, but the pathogenesis of glaucoma is not monofactorial. Among other factors, ischaemia and vascular dysregulation have been implicated in the mechanisms underlying glaucoma (Flammer et al. 2001). However, RNFL thinning is not specific for POAG and can be detected in various nonglaucomatous optic neuropathies, which may be confused with glaucoma. This holds true, for example, for nonarteritic anterior ischaemic optic neuropathy (NAION).

Nonarteritic anterior ischaemic optic neuropathy (NAION) is an acute ischaemic disorder of the optic nerve head, characterized by sudden loss of vision, optic disc oedema with resolution over weeks, visual field defects and, ultimately, optic disc pallor, altered optic disc morphology and decreased RNFL in a chronic disease stage (Hayreh 2009; Danesh-Meyer et al. 2001). An additional important finding noted in previous studies was that patients with NAION had a pale neuroretinal rim, whereas in POAG the remaining rim was most often pink (Danesh-Meyer et al. 2001; Quigley & Anderson 1977). The association of NAION with absent or a small cup/disc ratio (C/D) has been reported by several studies since 1974 (Hayreh 1974; Beck et al. 1984; Feit et al. 1984; Doro & Lessell 1985; Beck et al. 1987; Jonas et al. 1988; Burde 1993; Jonas & Xu 1993; Danesh-Meyer et al. 2001, 2005; Saito et al. 2006; Hayreh & Zimmerman 2008; You et al. 2009; Chan et al. 2009; Saito et al. 2008).

For ages, the gold standard for assessing the optic nerve head for changes has been disc photography. But photographic interpretation is both qualitative and subjective. In recent years, imaging devices such as laser scanning polarimetry and ultimately spectral domain optical coherence tomography (SD-OCT) have been introduced and are now used in daily clinical routine for diagnosis and monitoring of ONH diseases. Spectral domain optical coherence tomography is a noninvasive imaging technique that generates high-resolution cross-sectional images of transparent and translucent samples (Huang et al. 1991; Bouma & Tearney 2002; Fercher et al. 2003). Cirrus® and Spectralis® SD-OCT provide depth-resolved images of the retina and ONH, and with the use of spectral domain techniques, three-dimensional (3D) volumes can be imaged within a few seconds (Nassif et al. 2004; Schmidt-Erfurth et al. 2005). For the Spectralis® OCT, we used a new software, integrated in a new glaucoma module which has been introduced recently. Its advantage is precise and anatomically accurate diagnostic information. Until now, no study investigated NAION patients in comparison with POAG patients using this new measurement module.

We have used this measurement technique, to directly compare the effects of NAION and POAG compared with healthy age-matched subjects on ONH morphology and RNFL thickness measured with two different OCT machines. A comparison of the performance of the two OCT machines in this regard was made.

Subjects and Methods

Subjects

Twenty patients with moderate to severe POAG, 20 patients with NAION and 20 age-matched healthy subjects were included. The study protocol was approved by the Ethics Committee of the Medical University of Vienna and followed the guidelines of Good Clinical Practice and the Declaration of Helsinki. The nature of the study was explained, and written informed consent was obtained for all subjects included.

Inclusion and exclusion criteria

Inclusion criteria for patients with glaucoma were suspect appearance of the ONH of at least one eye (either large excavation >0.5, or asymmetry of excavation >0.2, or localized rim loss, or failure of ISNT rule, or baring of circumlinear vessels) and reproducible pathologic visual fields (VF) in standard automated perimetry (SAP) (either pathologic glaucoma hemifield test or a cluster of 3 points in pattern deviation plot significant at 0.5% not located at the border of the VF). The VF defect had to be compatible with glaucoma and specifically with the appearance of the optic disc, and the mean defect (MD) had to be between −6 and −15 decibel.

Diagnosis of NAION was made by two experienced neuro-ophthalmologist (AR and KK) of our department based on clinical examination and history and inclusion into the study was carried out >6 months after the acute disease onset. Nonarteritic anterior ischaemic optic neuropathy (NAION) diagnosis criteria were an acute, monocular painless visual loss together with ONH swelling and haemorrhage. Inclusion was only possible after the acute ONH oedema had subsided, and the optic disc borders were clearly delineated. Exclusion criteria were bilateral NAION, any finding indicative of arteritic AION (for criteria see Beck et al. 1987) or any other neuro-ophthalmologic pathology of the optic nerve. Again, the MD of the VF examination had to be between −6 and −15 dB, and VF measurements were matched between the two patient groups, NAION and POAG regarding MD and localization (the hemisphere) of the visual field defect.

Inclusion criteria for the healthy control subjects were normal appearance of the ONH, normal visual fields and intraocular pressure (IOP) and absence of any significant retinal pathology. Normal limits for IOP were defined as <21 mmHg and an abnormal visual field was defined either pathologic glaucoma hemifield test or a cluster of 3 points in pattern deviation plot significant at 0.5% not located at the border of the VF. Healthy controls were age-matched with the two patient groups.

We excluded all subjects with any evidence of other ocular pathology, history of ocular trauma or intraocular surgery within the last 6 months, ocular inflammation or infection within the last 3 months, astigmatism more than +2.0 dioptres and ametropia of more than ±5.0 dioptres. Optical coherence tomography (OCT) images with insufficient measurement quality (Quality score <6) were excluded.

Experimental paradigm

Initially, a complete ophthalmological examination was performed, including medical history, best-corrected Snellen visual acuity (VA), slit lamp examination, fundoscopy, measurement of IOP by Goldmann applanation tonometry and VF examination.

Subjects eligible for participating in the study according to the inclusion/exclusion criteria were included. If both eyes were includable, one eye was selected randomly.

The study was performed at the Department of Ophthalmology and Optometry of the Medical University of Vienna.

Methods

Automated visual field testing was performed with the Humphrey field analyser II (program 30-2). Visual field eligibility criteria were less than 33% false-positive responses, less than 33% false-negative responses and less than 33% fixation losses.

Cirrus® SD-OCT (Carl Zeiss Meditec, Dublin, CA, USA) measurements centred on ONH were performed by one technician, using the optic disc cube 200 × 200. With this program, a data cube of 6 mm square, which acquires as a series of 200 horizontal scan lines, each composed of 200 A-scans, was recorded. Measurements of the ONH parameters were automatically generated by a Carl Zeiss Meditec ONH analysis algorithm developed for Cirrus® SD-OCT (software version 5.0.0.326) without interaction of the technician. The algorithm identifies the termination of Bruch's membrane opening (BMO) as the ONH outer border, and the rim width is quantified as the thickness of the neuroretinal tissue as it turns to exit through the opening in Bruch's membrane, yielding a single area measurement in the ONH plane (Mwanza et al. 2011). According to Carl Zeiss Meditec, the computer algorithm minimizes the area of the trapezoids enclosed by consecutive scan radii on the sides, their intersections with the BMO on the proximal and those with the internal limiting membrane (ILM) at the outer boundary. Image quality was defined as an adequate signal strength >6. The RNFL was measured at a 3.4-mm-diameter circle around the ONH. For both parameters, the software calculates the average, superior, nasal, inferior and temporal quadrant values.

Another SD-OCT measurement was performed using the Spectralis® OCT Multicolor (Heidelberg Engineering, Heidelberg, Germany) to obtain measurements of the peripapillary RNFL as well as ONH parameters. For technical details, see Chauhan et al. 2013. Briefly, the Spectralis® OCT neuroretinal rim parameter (Bruch's membrane opening-minimum rim width = BMO-MRW) is defined as the minimum distance between the BMO and ILM (Fig. 1). It is a measurement from the actual anatomic outer border of the ONH, the BMO, and it is a geometrically accurate measurement as it accounts for its variable orientation. Bruch's membrane opening-minimum rim width (BMO-MRW) was computed at the 48 equally spaced angular positions around the BMO centre as means globally and for the four 45-degree sectors (superonasal, superotemporal, inferonasal and inferotemporal) and the two 90-degree sectors (nasal and temporal). The RNFL Spectralis® protocol generates a map showing the average thickness and six sector thicknesses (superonasal, nasal, inferonasal, inferotemporal, temporal and superotemporal in the clockwise direction for the right eye and counterclockwise for the left eye) at all 768 points registered during circular 3.4 mm diameter peripapillary scan acquisition. Spectralis® software version 1.9.9.0 was used.

Statistical methods

All statistical analyses were performed using the SPSS software package (version 21; SPSS, Inc., Chicago, IL, USA). p values <0.05 were considered as level of significance.

We used one-way ANOVA, analysis of variance for the comparison of RNFL and ONH parameters between healthy subjects, NAION and POAG patients, followed by post hoc *t*-tests.

Stepwise multiple linear regression analysis of the rim-RNFL correlation in healthy subjects and patients with glaucoma was performed including possible confounders, as age and disc area. We used the rim values as dependent variables and the RNFL values, age and disc area as independent variables. This analysis was performed separately for the global rim and RNFL values as well as for rim and RNFL values of four sectors for the Cirrus® OCT and six sectors for the Spectralis® OCT, respectively. Using the above-selected regression formulas, we tested whether the individual rim values were outside the 95% prediction interval. For the sectorial analysis, eyes were determined to be outside the limit when at least 1 sector was outside the 95% prediction interval.

We then determined the difference in global and sectorial ONH parameters from the expected values as calculated by the above-determined regression formulas. The areas under receiver

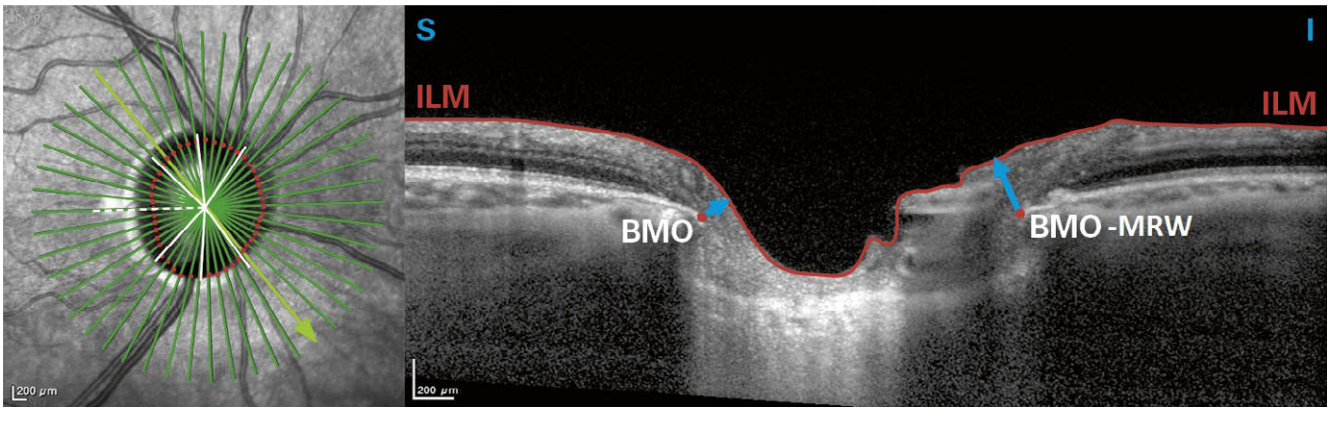

Fig. 1. Illustration of Bruch's membrane opening (BMO) = dot, the internal limiting membrane (ILM) = surface line and Bruch's membrane opening-minimum rim width (BMO-MRW) = arrow, which is the minimum distance from BMO to the ILM (Spectralis® OCT).

operating characteristics (AUROCs) for the global differences, measured with Spectralis® OCT and with Cirrus® OCT, as well as for the maximum of the sectorial differences to detect NAION among patients with POAG were calculated too. The receiver operating characteristic curve (ROC) plots the proportion of false positives (1-specificity) against the proportion of true positives (sensitivity). The diagnostic performance of the test is then judged, which is described quantitatively by reporting the AUROCs.

Results

From the 79 Caucasian subjects screened, 19 had to be excluded due to insufficient image quality and/or retinal pathologies (e.g. vitreomacular traction). A total of 60 subjects (20 healthy control subjects, 20 NAION and 20 POAG patients) were included. For subjects' baseline demographics, see Table 1. Mean disease duration of NAION patients was 52.7 ± 31.4 months (range: 18–138 months).

ANOVA showed statistically significant differences between groups for global RNFL and optic disc parameters ($p < 0.001$), measured with Spectralis® as well as Cirrus® OCT. Both glaucoma and NAION patients showed significantly smaller global RNFL thickness values compared to healthy subjects in *t*-tests ($p < 0.001$), while only the patients with glaucoma showed significantly smaller global BMO-MRW values for Spectralis® and global neuroretinal rim values for Cirrus® OCT compared to healthy controls ($p < 0.001$), (Table 2). Furthermore, the NAION patients showed significantly larger global BMO-MRW values for Spectralis® and global neuroretinal rim values for Cirrus® OCT compared to patients with glaucoma ($p < 0.001$). (Fig. 2)

The global BMO-based ONH parameters, measured with the two different OCT machines, showed a statistically significant correlation ($r = 0.93$), whereas in *t*-test a statistically significant difference between the two machines was detected ($p < 0.001$). The same results could be verified for the global RNFL parameters, with a statistically significant correlation ($r = 0.57$) between the two OCT machines, and again, in *t*-test, there was a statistically significant difference between the two machines ($p < 0.001$).

In the linear stepwise regression approach, for the Cirrus® and Spectralis® OCT measured global ONH parameters, disc size and RNFL were included as significant explanatory variables (Table 3). Using this regression formula, 9 NAION, 0 POAG and 1 healthy control subject for Cirrus® OCT and 12 NAION, 0 POAG and 1 healthy control subject for Spectralis® OCT had a global ONH parameter above the 95% confidence interval (CI), meaning that the ONH displayed a larger global rim width than expected. The results of the stepwise linear regression analysis of the sectorwise data are presented in Table 3. When applying the sectorwise stepwise linear regression formulas, eyes were determined to be outside the limit when at least one sector was outside the 95% prediction interval. This held true for 10 NAION, 0 POAG and three healthy control subject for Cirrus® OCT and for 15 NAION, one POAG and five healthy control subject for Spectralis® OCT. Stepwise linear regression analysis for global ONH parameters showed that age as covariable did not significantly contribute to this relationship for the Cirrus® as well as Spectralis® OCT, except for the temporal sector for the Spectralis® OCT.

The AUROC for the difference in the ONH parameters from their expected values to detect NAION among glaucoma measured with Spectralis® OCT (global BMO-MRW values) and with Cirrus® OCT (global neuroretinal rim values) was 0.980, and 0.945, respectively. For Spectralis® OCT to detect NAION among patients with POAG, sensitivity was 90% with a corresponding specificity of 95% (cut-off global difference between BMO-MRW and expected value >55.3 μm), whereas for Cirrus® OCT, sensitivity values of 80% and specificity values of 95% could have been reached (cut-off global difference between neuroretinal rim value and expected value >121.9 μm) (Fig. 3). The AUROC to detect NAION among patients with glaucoma measured with Spectralis® and the Cirrus® OCT, using the maximum differences in the sectorial values, was 0.978 and 0.958 (data not shown).

Discussion

In the present study, significant differences in RNFL and ONH parameters between POAG, NAION patient and healthy controls could be verified and NAION eyes were well discriminated from POAG using the difference in ONH parameters.

In a Japanese population, significant differences in ONH parameters between NAION and POAG eyes were found measured with Heidelberg Retina Tomograph (HRT). Cup area, C/D ratio and mean cup depth were significantly smaller, and the cup shape measure more negative, in NAION eyes than in POAG eyes ($p < 0.001$), whereas rim area was significantly

Table 1. Baseline demographics of the three subject groups described as mean values ± standard deviation

	Age (years)	Sex (female/male)	MD (decibel)	IOP (mmHg) on the study day	Spherical equivalent (dioptres)	Axial length (mm)	BMO area (mm^2) Spectralis® OCT
Healthy subjects N = 20	65.5 ± 8.1	9/11	−0.63 ± 1.52	15.1 ± 2.4	−0.28 ± 1.81	23.7 ± 0.8	1.85 ± 0.44
POAG patients N = 20	71.2 ± 6.0	11/9	−10.24* ± 4.71	15.5 ± 3.0	−0.61 ± 2.10	23.9 ± 1.2	2.11 ± 0.35
NAION patients N = 20	66.8 ± 8.3	8/12	−9.85* ± 4.79	13.6 ± 2.2	0.24 ± 1.39	23.25 ± 1.1	2.04 ± 0.39
p value of ANOVA	0.051		0.000	0.054	0.325	0.142	0.108

* Statistically significant difference in post hoc *t*-tests compared to healthy subjects.

Table 2. Mean values ± standard deviation of RNFL and ONH values of the three subject groups measured with Spectralis® OCT and Cirrus® OCT

Spectralis® OCT	Healthy subjects	POAG patients	NAION patients	p value of ANOVA*
Global RNFL (μm)	97.4 ± 8.0	64.3 ± 14.8†	63.7 ± 15.5†	<0.001
Temporal RNFL (μm)	65.9 ± 10.2	54.2 ± 14.6†	47.9 ± 15.5†	<0.001
Temporal superior RNFL (μm)	125.1 ± 23.5	75.3 ± 28.9†	70.7 ± 37.2†	<0.001
Nasal superior RNFL (μm)	117.8 ± 17.6	76.9 ± 24.4†	65.9 ± 28.0†	<0.001
Nasal RNFL (μm)	78.9 ± 13.3	52.9 ± 18.2†	48.9 ± 17.6†	<0.001
Nasal Inferior RNFL (μm)	121.0 ± 26.3	73.5 ± 19.1†	86.1 ± 31.8†	<0.001
Temporal inferior RNFL (μm)	147.8 ± 17.8	87.3 ± 34.3†	108.9 ± 46.6†	<0.001
Global BMO-MRW (μm)	339.4 ± 52.4	159.0 ± 45.8†	300.5 ± 62.3‡	<0.001
Temporal BMO-MRW (μm)	239.9 ± 45.4	128.4 ± 41.8†	241.6 ± 58.7‡	<0.001
Temporal superior BMO-MRW (μm)	314.0 ± 52.8	131.6 ± 61.0†	266.8 ± 86.9‡	<0.001
Nasal superior BMO-MRW (μm)	381.2 ± 74.6	178.7 ± 58.5†	320.2 ± 93.8‡†	<0.001
Nasal BMO-MRW (μm)	383.7 ± 61.9	176.2 ± 63.2†	317.9 ± 73.7‡†	<0.001
Nasal inferior BMO-MRW (μm)	416.2 ± 80.3	198.7 ± 66.4†	373.5 ± 96.2‡	<0.001
Temporal inferior BMO-MRW (μm)	347.7 ± 84.8	148.5 ± 75.3†	326.3 ± 101.4‡	<0.001
Cirrus® OCT	**Healthy subjects**	**POAG patients**	**NAION patients**	**p value of ANOVA§**
Global RNFL (μm)	91.9 ± 9.1	68.7 ± 11.1†	69.7 ± 11.4†	<0.001
Temporal quadrant RNFL (μm)	61.4 ± 11.1	52.6 ± 12.6†	52.7 ± 10.9	0.027
Superior quadrant RNFL (μm)	114.7 ± 12.4	78.7 ± 18.5†	73.9 ± 24.2†	<0.001
Nasal quadrant RNFL (μm)	69.8 ± 10.5	64.3 ± 8.1	61.3 ± 8.7†	0.019
Inferior quadrant RNFL (μm)	121.6 ± 18.9	77.1 ± 15.7†	90.6 ± 25.7†	<0.001
Global neuroretinal rim (μm)	429.9 ± 82.1	167.1 ± 33.7†	416.12 ± 78.3‡	<0.001
Temporal quadrant neuroretinal rim (μm)	308.3 ± 133.3	116.8 ± 59.1†	309.0 ± 140.2‡	<0.001
Superior quadrant neuroretinal rim (μm)	419.1 ± 124.7	161.6 ± 68.3†	380.4 ± 170.6‡	<0.001
Nasal quadrant neuroretinal rim (μm)	536.8 ± 157.9	209.5 ± 144.4†	515.7 ± 149.6‡	<0.001
Inferior quadrant neuroretinal rim (μm)	455.3 ± 133.9	180.6 ± 75.0†	459.4 ± 167.7‡	<0.001

* Based on ANOVA, analysis of variance, comparison of healthy subjects, NAION and POAG patients.
† Post hoc *t*-test comparing with healthy group $p < 0.05$.
‡ Post hoc *t*-test comparing with POAG group $p < 0.05$.

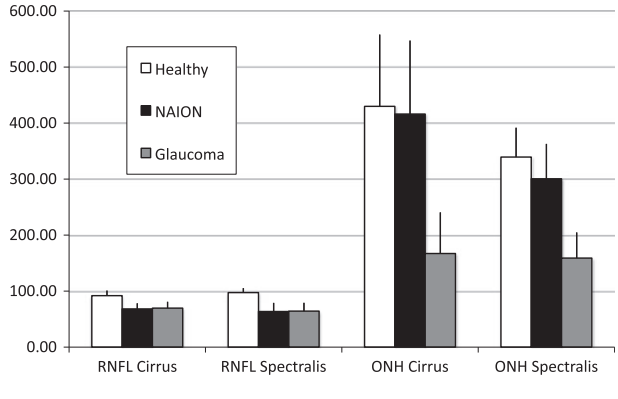

Fig. 2. Global Bruch's membrane opening (BMO)-based optic nerve head (ONH) values measured with Spectralis® OCT and Cirrus® OCT in the patient groups (NAION and POAG) and healthy controls.

greater. Furthermore, NAION eyes had smaller disc areas than control eyes (Saito et al. 2006, 2008). To the same conclusion came Danesh-Meyer et al. (2010) where POAG eyes had larger, deeper cups, smaller rims, more cup volume and less rim volume compared to NAION eyes as measured with HRT2. In this study, RNFL thickness measured with time domain (TD) optical coherence tomography (Stratus OCT; Carl Zeiss Meditec, Inc., Dublin, CA) was greater at the same visual field mean deviation (MD) for NAION compared with POAG. Diagnosis of glaucoma consists of different factors, which are limited through variability and are partly under subjective influence, as for example the visual field examination and the clinical determination of the C/D ratio through the physician (Cox & O'Brien 1992). Imaging of the ONH and RNFL has the advantages of objectivity and reproducibility. However, RNFL thinning is not specific for POAG and nonglaucomatous diseases such as NAION, retinal diseases and compressive optic neuropathy can cause RNFL thinning as well, leading possibly to wrong diagnoses.

Recent advances in the technology of OCT allow accurate measurements of retinal and ONH structures. Reis et al. 2012; have concluded that the optic disc margin-based neuroretinal rim assessment lacks a justifiable anatomic and geometric rationale. That is why, a new parameter, the BMO-MRW, was introduced and was proven as a measurement from an anatomically accurate border of the rim that also takes into account its varying trajectory relative to the point of measurement. Chauhan et al. (2013) could prove that BMO-MRW had a better diagnostic performance compared with current confocal scanning laser tomography or other SD-OCT–based ONH and RNFL parameters.

In the present study, a significant difference in ONH parameters between POAG and NAION patients could be

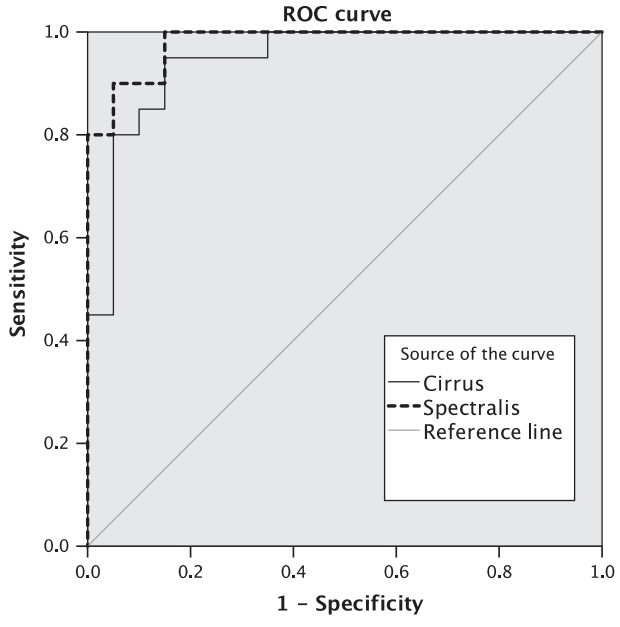

Fig. 3. Operating characteristic curve (ROC) curve for the difference in the optic disc parameters from their expected values—as determined by the multiple linear regression formula—for Spectralis® OCT = global BMO-MRW values and Cirrus® OCT = global neuroretinal rim values

verified with SD-OCT, while the circumpapillary RNFL was similarly reduced in both groups compared to healthy controls. With the present data, we are able to show that the different impact of NAION and POAG on the BMO-based parameters versus the circumpapillary RNFL may be exploited to differentiate between the two disease entities. This, in a clinical setting, can be challenging, especially in the chronic disease stage when diagnosis is missing or former medical records are not available. We found essentially the same results with both OCT machines the Spectralis® and the Cirrus® OCT. The correlation between the two global BMO-based ONH parameters was highly statistically significant ($r = 0.93$), whereas in *t*-test a statistically significant difference between the two machines was detected ($p < 0.001$). The reasons for this might be the different delineation of the anatomic structures, different calculation models, as well as the diverse scaling methods of both of the instruments. To evaluate the diagnostic power of OCT ONH measurements to differentiate POAG from NAION, a stepwise linear regression analysis of the rim-RNFL correlation with adjusting covariates (optic disc area and age) was performed. Based on the regression formula, the AUROC was calculated to test the discrimination between glaucoma and NAION. Stepwise linear regression analysis revealed an influence of the disc size on the relation between RNFL and the ONH parameter for both devices. Area under the receiver operator characteristic (AUROC) revealed a similarly good discrimination between glaucoma and NAION for Spectralis® (0.980) and Cirrus® OCT (0.945).

Our study has several limitations. A major issue is the small sample size, but that is in line with prior studies. However, given the very significant results observed between the groups, a generalization of the study results can be carried out. But, our results may not automatically be generalized to any other cause of optic nerve damage. An increased excavation of the ONH combined with a decline of RNFL may be present in some nonglaucomatous diseases, such as arteritic AION, diabetes and compressive optic neuropathy (Takahashi et al. 2006; Danesh-Meyer et al. 2008; Chan et al. 2009). Further research comparing these diseases with glaucoma may be warranted

In conclusion, the data provided here show that BMO-based OCT measurements of the ONH together with RNFL thickness might be an objective way to distinguish POAG from NAION and that none of the two OCT instruments used performed better in this respect.

Table 3. Linear stepwise regression analysis of confounders (age, disc size and RNFL) on ONH parameters

ONH parameters	B RNFL	B Disc size	B Age	Intercept	R^2	p
Spectralis® global	4.148	−0.062		37.578	0.792	<0.001
Spectralis® temporal	1.976		−2.680	247.852	0.313	=0.001
Spectralis® temporal superior	2.385			−16.107	0.637	<0.001
Spectralis® nasal superior	2.724	−0.093		198.808	0.602	<0.001
Spectralis® nasal	3.567	−0.122		286.935	0.572	<0.001
Spectralis® nasal inferior	3.089	−0.103		211.304	0.691	<0.001
Spectralis® temporal inferior	2.389			−32.734	0.579	<0.001
Cirrus® global	6.916	−192.734		92.859	0.518	<0.001
Cirrus® temporal						
Cirrus® superior	4.610	−122.242		68.353	0.585	<0.001
Cirrus® nasal	7.637	−319.879		446.785	0.246	0.005
Cirrus® inferior	4.196	−151.493		178.326	0.563	<0.001

B = unstandardized regression coefficient; R^2 = squared correlation.

References

Beck RW, Savino PJ, Repka MX, Schatz NJ & Sergott RC (1984): Optic disc structure in anterior ischemic optic neuropathy. Ophthalmology **91**: 1334–1337.

Beck RW, Servais GE & Hayreh SS (1987): Anterior ischemic optic neuropathy. IX. Cup-to-disc ratio and its role in pathogenesis. Ophthalmology **94**: 1503–1508.

Bouma BE & Tearney GJ (2002): Handbook of Optical Coherence Tomography. New York, NY: Marcel Dekker.

Burde RM (1993): Optic disk risk factors for nonarteritic anterior ischemic optic neuropathy. Am J Ophthalmol **116**: 759–764.

Chan CK, Cheng AC, Leung CK, Cheung CY, Yung A, Gong B & Lam DS (2009): Quantitative assessment of optic nerve head morphology and retinal nerve fibre layer in non-arteritic anterior ischaemic optic neuropathy with optical coherence tomography and confocal scanning laser ophthalmoloscopy. Br J Ophthalmol **93**: 731–735.

Chauhan BC, O'Leary N, Almobarak FA, et al. (2013): Enhanced detection of open-angle glaucoma with an anatomically accurate optical coherence tomography-derived neuroretinal rim parameter. Ophthalmology **120**: 535–543.

Cox MJ & O'Brien C (1992): Comparison of computer-assisted versus manual optic nerve head pallor measurement. Invest Ophthalmol Vis Sci **33**: 3169–3173.

Danesh-Meyer HV, Savino PJ & Sergott RC (2001): The prevalence of cupping in end-stage arteritic and nonarteritic anterior ischemic optic neuropathy. Ophthalmology **108**: 593–598.

Danesh-Meyer H, Savino PJ, Spaeth GL & Gamble GD (2005): Comparison of arteritis and nonarteritic anterior ischemic optic neuropathies with the Heidelberg Retina Tomograph. Ophthalmology **112**: 1104–1112.

Danesh-Meyer HV, Papchenko T, Savino PJ, Law A, Evans J & Gamble GD (2008): *In vivo* retinal nerve fiber layer thickness measured by optical coherence tomography predicts visual recovery after surgery for parachiasmal tumors. Invest Ophthalmol Vis Sci **49**: 1879–1885.

Danesh-Meyer HV, Boland MV, Savino PJ, Miller NR, Subramanian PS, Girkin CA & Quigley HA (2010): Optic disc morphology in open-angle glaucoma compared with anterior ischemic optic neuropathies. Invest Ophthalmol Vis Sci **51**: 2003–2010.

Doro S & Lessell S (1985): Cup-disc ratio and ischemic optic neuropathy. Arch Ophthalmol **103**: 1143–1144.

Feit RH, Tomsak RL & Ellenberger C Jr (1984): Structural factors in the pathogenesis of ischemic optic neuropathy. Am J Ophthalmol **98**: 105–108.

Fercher AF, Drexler W, Hitzenberger CK & Lasser T (2003): Optical coherence tomography-principles and applications. Rep Progr Phys **66**: 239–303.

Flammer J, Pache M & Resink T (2001): Vasospasm, its role in the pathogenesis of diseases with particular reference to the eye. Prog Retin Eye Res **20**: 319–349.

Hayreh SS (1974): Pathogenesis of cupping of the optic disc. Br J Ophthalmol **58**: 863–876.

Hayreh SS (2009): Ischemic optic neuropathy. Prog Retin Eye Res **28**: 34–62.

Hayreh SS & Zimmerman MB (2008): Nonarteritic anterior ischemic optic neuropathy: refractive error and its relationship to cup/disc ratio. Ophthalmology **115**: 2275–2281.

Huang D, Swanson EA, Lin CP, et al. (1991): Optical coherence tomography. Science **254**: 1178–1181.

Jonas JB & Xu L (1993): Optic disc morphology in eyes after nonarteritic anterior ischemic optic neuropathy. Invest Ophthalmol Vis Sci **34**: 2260–2265.

Jonas JB, Gusek GC & Naumann GO (1988): Anterior ischemic optic neuropathy: nonarteritic form in small and giant cell arteritis in normal sized optic discs. Int Ophthalmol **12**: 119–125.

Leung CK, Medeiros FA, Zangwill LM, et al. (2007): American Chinese glaucoma imaging study: a comparison of the optic disc and retinal nerve fiber layer in detecting glaucomatous damage. Invest Ophthalmol Vis Sci **48**: 2644–2652.

Medeiros FA, Vizzeri G, Zangwill LM, Alencar LM, Sample PA & Weinreb RN (2008): Comparison of retinal nerve fiber layer and optic disc imaging for diagnosing glaucoma in patients suspected of having the disease. Ophthalmology **115**: 1340–1346.

Mwanza JC, Oakley JD, Budenz DL & Anderson DR (2011): Cirrus Optical Coherence Tomography Normative Database Study Group. Ability of cirrus HD-OCT optic nerve head parameters to discriminate normal from glaucomatous eyes. Ophthalmology **118**: 241–248.

Nassif N, Cense B, Park BH, Yun SH, Chen TC, Bouma BE, Tearney GJ & de Boer JF (2004): *In vivo* human retinal imaging by ultrahigh-speed spectral domain optical coherence tomography. Opt Lett **29**: 480–482.

Quigley HA & Anderson DR (1977): Cupping of the optic disc in ischemic optic neuropathy. Trans Sect Ophthalmol Am Acad Ophthalmol Otolaryngol **83**: 755–762.

Quigley HA, Addics EM & Green WR (1982): Optic nerve damage in human glaucoma, III: quantitative correlation of nerve fiber loss and visual field defect in glaucoma, ischemic neuropathy, papilledema, and toxic neuropathy. Arch Ophthalmol **100**: 135–146.

Reis AS, O'Leary N, Yang H, Sharpe GP, Nicolela MT, Burgoyne CF & Chauhan BC (2012): Influence of clinically invisible, but optical coherence tomography detected, optic disc margin anatomy on neuroretinal rim evaluation. Invest Ophthalmol Vis Sci **53**: 1852–1860.

Saito H, Tomidokoro A, Sugimoto E, Aihara M, Tomita G, Fujie K, Wakakura M & Araie M (2006): Optic disc topography and peripapillary retinal nerve fiber layer thickness in nonarteritic ischemic optic neuropathy and open-angle glaucoma. Ophthalmology **113**: 1340–1344.

Saito H, Tomidokoro A, Tomita G, Araie M & Wakakura M (2008): Optic disc and peripapillary morphology in unilateral nonarteritic anterior ischemic optic neuropathy and age- and refraction-matched normals. Ophthalmology **115**: 1585–1590.

Schmidt-Erfurth U, Leitgeb RA, Michels S, et al. (2005): Three-dimensional ultrahigh-resolution optical coherence tomography of macular diseases. Invest Ophthalmol Vis Sci **46**: 3393–3402.

Takahashi H, Goto T, Shoji T, Tanito M, Park M & Chihara E (2006): Diabetes-associated retinal nerve fiber damage evaluated with scanning laser polarimetry. Am J Ophthalmol **142**: 88–94.

You QS, Xu L, Wang YX & Jonas JB (2009): Frequency of non-arteritic anterior ischemic optic neuropathy in crowded optic discs: the Beijing Eye Study. Acta Ophthalmol **87**: 354–355.

Received on July 19th, 2017.
Accepted on April 1st, 2018.

Correspondence:
Clemens Vass, MD
Department of Ophthalmology and Optometry
Medical University of Vienna, General Hospital
Währinger Gürtel 18-20
A-1090 Vienna
Austria
Tel: +43-1-40400-79000
Fax: +43-1-40400-79020
Email: clemens.vass@meduniwien.ac.at

The first author and the corresponding author have full access to all the data in the study, take responsibility for the integrity of the data and the accuracy of the data analysis, and have conducted and were responsible for the data analysis.